Studying of photoluminescence characteristics of CdTe/ZnS QDs manipulated by TiO$_2$ inverse opal photonic crystals

Xiao-Chun Chi [a], Ying-Shu Yang [a], Ying-Hui Wang [a,*], Jie-Chao Gao [a], Ning Sui [a], Hai-Gui Yang [b], Lu Zou [a], Zhi-Hui Kang [a], Han-Zhuang Zhang [a,*]

[a] Key Laboratory of Physics and Technology for Advanced Batteries (Ministry of Education), College of Physics, Jilin University, Changchun 130012, PR China
[b] Key Laboratory of Optical System Advanced Manufacturing Technology, Changchun Institute of Optics, Fine Mechanics and Physics, Chinese Academy of Sciences, Changchun 130033, PR China

ABSTRACT

The photoluminescence (PL) characteristics of CdTe/ZnS quantum dots (QDs) infiltrated in TiO$_2$ inverse opal photonic crystals (PCs) are studied in detail. The PL dynamics of QDs show that the PCs could accelerate the PL relaxation rate of QDs as the PL peak of QDs is overlapped with the photonic stop band of PCs. Besides, the PCs could decrease the activation energy of QDs due to its porous structure and suppress the exciton annihilation process of QDs at high excitation intensity, owing to the light scattering effect. The final results are beneficial for people in further understanding the role of inverse opal PCs on manipulating the PL characteristics of QDs.

© 2015 Elsevier B.V. All rights reserved.

1. Introduction

Semiconductor quantum dots (QDs) are a kind of interesting novel nano-materials, which own many excellent properties [1], and could be used in the fields of optoelectronic devices [2] and biomedical imaging [3], etc. Among them, CdTe/ZnS quantum dots are a type of core–shell quantum dots, which exhibit excellent luminescent characteristics [4], and have potential applications in the fields of light-emitting diodes [2]. Generally speaking, the luminescence yield of QDs depends on the radiative and non-radiative process of excited QDs, which are sensitive to the surrounding environment, such as the reflective index [5] and the temperature [6]. If the environment of QDs could be changed, it would be possible to further manipulate the photoluminescence (PL) characteristics of device performance based on QDs, which also opens a window to broaden the applications of semiconductor QDs. Recently, the appearance of photonic crystal (PC) could resolve this problem [7–9], since it could change the environments in which light propagation is altered in the photonic stop band (PSB) of PCs [10,11]. Therefore, the PCs could manipulate the PL characteristics of luminescent species in PCs [12,13]. Generally, the three-dimensional (3D) TiO$_2$ inverse opal PCs own a high refractive index and exhibit an obvious effect on manipulating

the light propagation [14–20], which owns a huge potential to manipulate the PL characteristics of QDs [21–23]. However, the PC-dependent PL characteristics of QDs still remain limited and need to be further exploited.

In this work, the CdTe/ZnS QDs have been infiltrated in the 3D TiO$_2$ inverse opal PCs so as to study the PL characteristics of CdTe/ZnS QDs. The rich spectral data show that the PCs could improve the PL properties of QDs in many aspects through controlling the position of PSB in PCs and changing the environment temperature, the PL characteristics of QDs could be effectively manipulated, which is beneficial for individuals to further understand the excited state process of QDs.

2. Experimental

2.1. Material and methods

The concentration of CdTe/ZnS QDs (Janus New-Materials Co., Ltd) was 3 mg ml^{-1} and the size of CdTe/ZnS QDs was ~3 nm. The CdTe/ZnS QDs solution were infiltrated in TiO$_2$ opal inverse opal photonic crystals, so as to make sure that the optical density around the QDs has been influenced by TiO$_2$ opal inverse opal photonic crystals. Methyl methacrylate (MMA; Guangfu, Tianjin) were purified by sodium hydroxide solution before used.

Firstly, we used the vertical self-assembled deposition method to prepare 3D PMMA opal PCs [13]. After adding 1.5 mL PMMA latex into a small beaker, which was holding 20 mL deionized

* Corresponding authors. Tel.: +86 431 85167378; fax: +86 431 85166112.
E-mail addresses: yinghui_wang@jlu.edu.cn (Y.-H. Wang), zhanghz@jlu.edu.cn (H.-Z. Zhang).

water, we inserted three pieces of glass slides vertically into the beaker. Then we put the beaker in an electrothermal constant-temperature dry box and kept a constant temperature at 32 °C for about 24 h. After these steps, we could obtain 3D PMMA opal PCs. Secondly, we prepared the 3D TiO$_2$ inverse opal PCs based on 3D PMMA opal PCs according to reference [24]. We mixed the dibutyl phthalate and alcohol according to the volume ratio of 1:1. When stirring the mixture with a magnetic stirrer, we added a certain amount of concentrated nitric acid, which is following the step that we stirred the mixture for 2 h. Then we infiltrated the mixture in PMMA opal PCs. After putting the infiltrated PMMA opal PCs in Solid Tube Furnace, we calcined it at 500 °C for 3 h, and then we decrease the temperature to room temperature. Finally, we obtain the TiO$_2$ inverse opal PCs.

2.2. Measurement

Steady-state transmittance measurements were carried out using a UV–Vis spectrophotometer (Purkinje, TU-1810PC) at normal incidence. Photoluminescence (PL) spectra were recorded by a fiber optic spectrometer (Ocean Optics, USB4000) with a femtosecond laser pulse with excitation wavelength of 400 nm. The morphology of the samples was measured with a JEOL S-4800 field emission scanning electron microscope (FE-SEM). XRD measurement was performed by R-AXIS RAPID II (Rigaku). Time-correlated single-photon counting (TCSPC) measurement was performed by a fluorescence spectrometer (mini-τ, Edinburgh Photonics) equipped with an EPL405 laser diode.

3. Results and discussion

We prepared TiO$_2$ inverse opal PCs with two different PSBs which were named PC#1 and PC#2, respectively. Fig. 1(a) shows the SEM image of PC#1 which is presented in the vertical direction. It is clear that the PC#1 yields a long-range ordered hexagonal arrangement of inverse opal with the center-to-center distance of

~350 nm between the macro-pores on the plane of PC#1. From the side-view, the 3D image of PC#1 also exhibits that PC#1 is well-organized multilayer structure without cracks or defects, as seen in Fig. 1(b). Therefore, the PL characteristics of CdTe/ZnS QDs could be manipulated after they are infiltrated in 3D inverse opal PCs. The X-ray diffraction (XRD) pattern of the PC#1 was exhibited in Fig. 1(c), showing that it is tetragonal structure. Fig. 1(d) offers the transmittance spectra of TiO$_2$ inverse opal PCs at normal incidence, showing that PC#1 and PC#2 display obvious PSB, centering at ~515 and 620 nm, respectively. The PC#1 on the glass substrate shows green color and its color would become blue as the direction is changed, indicating that the PSB of PC#1 could change with the incident angle [6].

The absorption and fluorescence spectra of CdTe/ZnS QDs performed in aqueous solution in Fig. 2(a) manifests that the first absorption peak and the fluorescence maximum are located at ~480 and 520 nm, respectively. The emission peak of QDs (520 nm) is closed to the PSB of PC#1 (515 nm) and far away from that of PC#2 (620 nm), as shown in Figs. 1(b) and 2(a). This indicates that the PC#1 could influence the PL decay rate of QDs, but PC#2 could not. Actually, the PL decay rate of QDs is really accelerated by the PC#1 [24], as seen in Fig. 2(b). The decay process of CdTe/ZnS QDs shows an exponential relaxation behavior. Considering the location difference of CdTe/ZnS QDs in PCs, their corresponding PL decay traces influenced by PCs become very complicated. Therefore the total PL curves presented in Fig. 2(b) are fitted with a continuous distribution function of decay rates [25]:

$$I(t) = I(0) \int_{\gamma=0}^{\infty} \varphi(\gamma) \exp(-\gamma t) d\gamma \tag{1}$$

where $\varphi(\gamma)$ is a distribution of decay rates with dimension of time; $I(t)$ is the fluorescence intensity; $\varphi(\gamma)$ describes a distribution of the emitters' concentration with a certain γ, weighted by the corresponding γ_{rad} [26]. $\varphi(\gamma)$ is the long-normal distribution function as described below:

$$\varphi(\gamma) = A \exp[(-\ln^2(\gamma/\gamma_{MF}))/w^2] \tag{2}$$
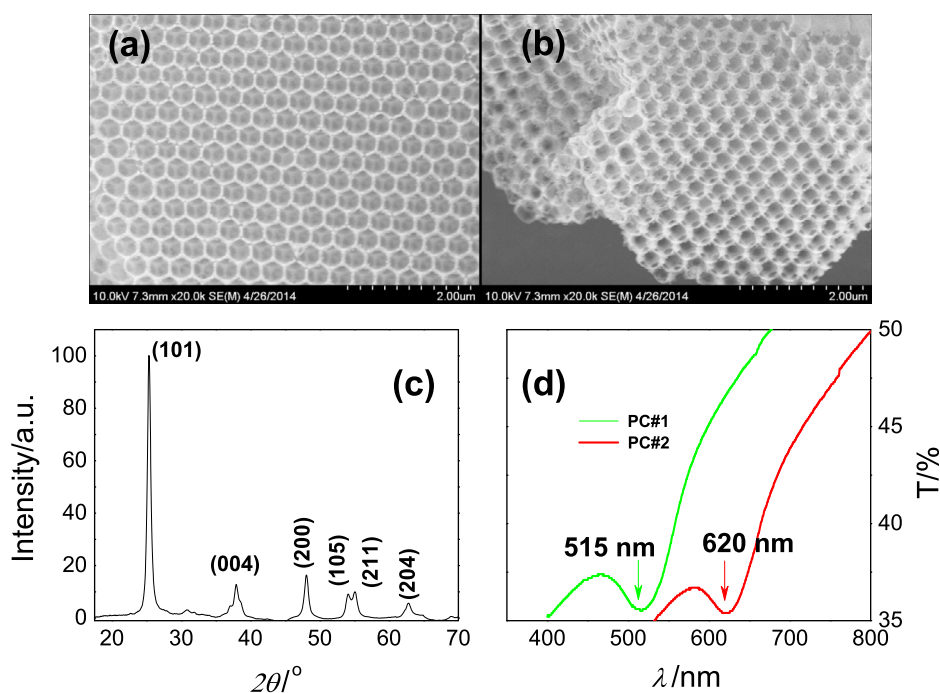
Fig. 1. SEM image of surface (a) and section (b) of TiO$_2$ inverse opal PCs; (c) the XRD patterns of TiO$_2$ inverse opal PCs; (d) transmittance spectra of TiO$_2$ inverse opal PCs.
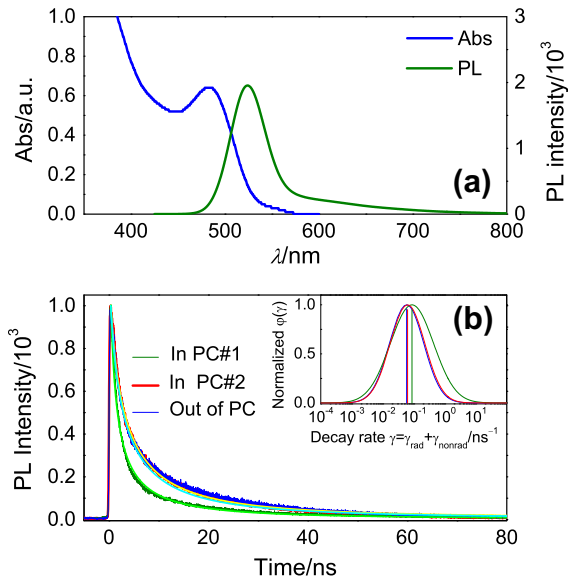
Fig. 2. (a) Normalized absorption and PL spectra of CdTe/ZnS QDs; (b) PL traces of CdTe/ZnS QDs in TiO$_2$ inverse opal PC#1, PC#2 and out of PCs. Inset: the corresponding decay-rate distributions for CdTe/ZnS QDs with different PSBs. $\Delta\gamma$ is 0.347 (out of PCs), 0.842 (in PC#1) and 0.379 (in PC#2) ns^{-1}, respectively.

where γ_{MF} is the most-frequency decay rate corresponding to the maximum of $\varphi(t)$; w is a dimensionless width parameter that determines the distribution width ($\Delta\gamma$) at $1/e$; A is the normalization constant, so that $\int\varphi(\gamma)d\gamma = 1$. The corresponding γ_{MF} of QDs in PC#2 (0.063 ns^{-1}) is similar to that out of PCs (0.059 ns^{-1}), which are both lower than that of QDs in PC#1 (0.088 ns^{-1}). Apparently, the manipulation of γ_{MF} is related to the position of PSB in PCs and the PL peak of luminescence species. Meanwhile, the distribution width could be calculated as described below:

$$\Delta\gamma = 2\gamma_{MF}\sinh w \tag{3}$$

The inset of Fig. 2(b) results show that the rate distribution width is 0.347 ns^{-1} (out of PCs), 0.842 (in PC#1) and 0.379 ns^{-1} (in PC#2), respectively, which becomes complex under the manipulation of PC#1. Herein, the difference between relaxation behaviors of CdTe/ZnS QDs in and out of PC#1 could be attributed to the variance of optical density round the luminescent species [24].

Fig. 3(a) exhibits the temperature-dependent PL spectra of CdTe/ZnS QDs out of PCs. The pure CdTe/ZnS QDs are excited by the femtosecond laser pulse with wavelength of 400 nm and the size of focused beam is 3 mm. As shown in Fig. 2(a), the Stokes shift of CdTe/ZnS QDs is small. When the QDs are excited by laser pulse with wavelength of 400 nm, the PL of QDs could not be influenced by the excitation pulse. The spectral data exhibits that the PL intensity gradually decreases with the temperature rising (as seen in Fig. 3(b)), which is assigned to the enhancement of nonradiative relaxation path [27]. The corresponding data are modeled by using the equation expressed as:

$$I(t) = I_0 \left[1 + C \exp\left(-\frac{E_a}{k_B T} \right) \right]^{-1} \tag{4}$$

where I_0 is initial integrated PL intensity (IPLI); E_a is the activation energy; C is constant; k_B is Boltzmann constant. The fitted results are shown as the solid lines, exhibiting that the activation energy E_a is 310 and 324 meV for CdTe/ZnS QDs in and out of PC#1, respectively. This indicates that the PC#1 with special porous structure effectively facilitates CdTe/ZnS QDs touching with the round environment and leads to the decrease of activation energy of QDs, since the touching area between CdTe/ZnS QDs (out of PCs) and the environment is limited and is smaller than that in PC#1.
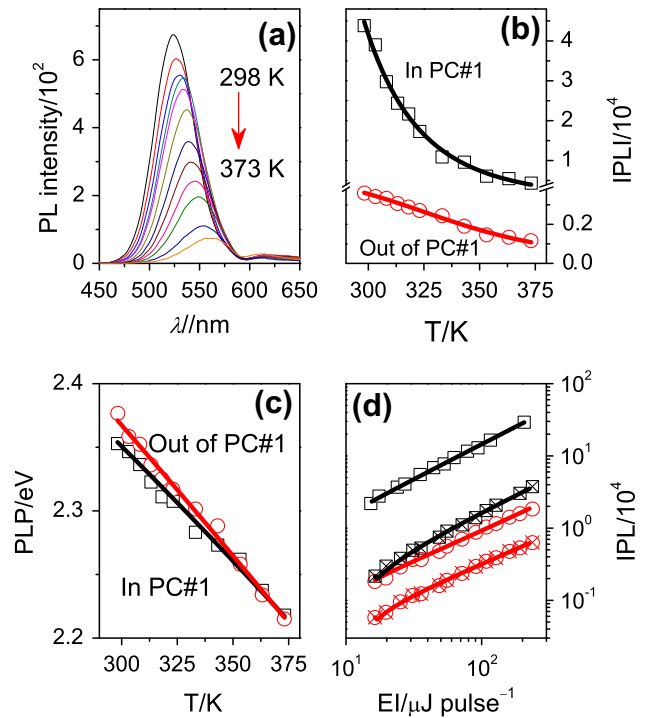
Fig. 3. (a) Temperature dependent of fluorescence spectra of CdTe/ZnS QDs in aggregation state (out of PCs); (b) temperature-dependent of integrated PL intensity (IPLI); (c) PL peak (PLP) of CdTe/ZnS QDs in and out of TiO$_2$ inverse opal PC#1; (d) excitation intensity-dependent integrated fluorescence intensity of CdTe/ZnS in and out of TiO$_2$ inverse opal PC#1. In Fig. 3. D, ($\square$), ($\bigcirc$), ($\boxtimes$) and ($\otimes$) reflect the excitation-dependent IPLI of CdTe/ZnS QDs in and out of TiO$_2$ inverse opal PC#1 at room temperature (293 K) and high temperature (373 K), respectively.

Therefore, the porous structure of PCs is mainly responsible for the variance of temperature-dependent IPLI (as shown in Fig. 3(b)). The IPLIs of QDs in PC#1 decreases faster than that of QDs out of PC, when temperature increases.

The PL peaks (PLP) of CdTe/ZnS QDs in and out of PC#1 as a function of temperature are also plotted in Fig. 3(c), which are consistent with the previous report [28]. They both red shift with temperature rising and exhibit different evolution processes. This phenomenon should be caused by a change in the relative position of the conduction and valence bands. The change could result from the dilatation of the lattice and the interaction of electrons with the lattice [29]. The corresponding data in Fig. 3(c) could be modeled by the Varshni relation [27]:

$$E_{PLP}(T) = E_{PLP}(0) - \alpha T^2 (T + \beta)^{-1} \tag{5}$$

where $E_{PLP}(T)$ is the PLP value as the function of absolute temperature T, $E_{PLP}(0)$ is the PLP value at 0 K, α is a temperature coefficient, and β is approximately the Debye temperature of the semiconductor. Eq. (5) is based on the temperature-dependent dilatation of lattice and the interaction between lattice phonon and exciton [30]. Finally, it is found that the $E_{PLP}(0)$ is 2.68 and 2.79 eV (in and out of PC#1); α is 2.6×10^{-3} and 2.5×10^{-3} eV K^{-1} (in and out of PC#1); and β is 402 and 222 K (in and out of PC#1). Herein, the difference of $E_{PLP}(0)$ should be attributed to two reasons. The first one is the porous structure of PC#1, which is able to break the aggregation among CdTe/ZnS QDs and suppresses the self-absorption and energy transfer among QDs; the second one is the PSB of PC#1 which could influence the PL spectra through changing the optical density round the CdTe/ZnS QDs. Meanwhile, the porous structure of PC#1 could influence the variance of α and β as the temperature rising, since the thermal exchange process between CdTe/ZnS QDs and the environment could be much effectively in PC#1.

The pulse excitation intensity-dependent IPLIs of CdTe/ZnS QDs in and out of PC#1 at room temperature (293 K) and high temperature (373 K) are compared in Fig. 3(d). In logarithmic coordinates, their IPLIs approximately linearly enhance with the laser intensity increasing, no matter the QDs are at room temperature or high temperature. However, the corresponding slopes are sensitive to the PCs and the temperature. In order to clarify the role of PC#1 and the temperature on the IPLI enhancement process, the PL data in Fig. 3(d) are fitted by using function of $I_{IPLI} \propto (I_{EI})^{\alpha}$, I_{IPLI} and I_{EI} are the IPLI and the excitation intensity, respectively. Finally, it is found that α is 0.96 (in PC#1) and 0.89 (out of PC#1) at 292 K, and 0.92 (in PC#1) and 0.82 (out of PC#1) at 373 K. Since the bandwidth of laser pulse is ~200 fs, which is too short to generate the thermal accumulation effect. Since the thermal accumulation effect is eliminated, the exciton annihilation (Auger recombination [31,32]) originated from the high excitation intensity could be responsible for the PL enhancement nonlinearity of CdTe/ZnS QDs.

As the CdTe/ZnS QDs are infiltrated in TiO$_2$ inverse opal PCs, the scattering effect of PCs could make many more CdTe/ZnS QDs around the excitation regime absorb photons and decrease the photon density on each CdTe/ZnS QDs, which decrease the probability of exciton annihilation occurring in CdTe/ZnS QDs in TiO$_2$ inverse opal PCs at high excitation intensity. When the CdTe/ZnS QDs aggregate together, the exciton annihilation could easily happen after the QDs are excited by femtosecond laser. Therefore, α in PC#1 (0.96) is closed to 1 in comparison with that out of PC#1 (0.89). When the temperature rises, the activity of excitons in QDs increases, which accelerates the collision annihilation process of excitons in QDs. Accordingly, the value of α could decrease at high temperature (373 K), no matter the CdTe/ZnS QDs are in or out of PC#1. The light scattering of inverse opal PCs is still effective at high temperature, therefore α of CdTe/ZnS QDs in PC#1 (0.92) is still larger than that out of PC#1 (0.82) at 373 K.

4. Conclusions

The PL characteristics of CdTe/ZnS QDs infiltrated in TiO$_2$ inverse opal photonic crystals (PCs) are systemically studied. The PL relaxation rate of CdTe/ZnS QDs could be accelerated if its PL peak is overlapped with the PSB of PCs. Meanwhile, it was found that the porous structure of TiO$_2$ inverse opal PCs decrease the activation energy of CdTe/ZnS and facilitate the thermal exchange process, which could enhance the PL loss of CdTe/ZnS QDs at high temperature. When the intensity of femtosecond laser pulse increases, it is found that the light scattering effect originated from the inverse opal PCs suppress the PL enhancement nonlinearity of CdTe/ZnS QDs through decreasing the exciton annihilation process occurring in CdTe/ZnS QDs. The final results are beneficial for people to further understand the role of inverse opal PCs on the PL characteristics of QDs. In the future, the PCs could be applied in the optoelectronic fields, such as light-emitted diode, dye sensitized solar cells and optical sensor devices duo to its excellent optical properties. This could further facilitate the development of optoelectronic devices and accelerate their industrialization.

References

[1] A.D. Yoffe, Semiconductor quantum dots and related systems, electronic, optical, luminescence and related properties of low dimensional systems, Adv. Phys. 50 (2001) 1–208.

[2] Q.J. Sun, Y.A. Wang, L.S. Li, D.Y. Wang, T. Zhu, J. Xu, C.H. Yang, Y.F. Li, Bright, multicoloured light-emitting diodes based on quantum dots, Nat. Photon. 1 (2007) 717–722.

[3] Y.T. Lim, S. Kim, A. Nakayama, N.E. Stott, M.G. Bawendi, J.V. Frangioni, Selection of quantum dot wavelengths for biomedical assays and imaging, Mol. Imag. 2 (2003) 50–64.

[4] Y.F. Liu, J.S. Yu, Insitu synthesis of highly luminescent glutathione-capped CdTe/ZnS quantum dots with biocompatibility, J. Colloid Inter. Sci. 351 (2010) 1–9.

[5] Y.S. Zhu, W. Xu, H.Z. Zhang, W. Wang, L. Tong, S. Xu, Z.P. Sun, H.W. Song, Highly modified spontaneous emissions in YVO$_4$:Er^{3+} inverse opal and refractive index sensing application, Appl. Phys. Lett. 100 (2012) 081104.

[6] Y.S. Zhu, W. Xu, H.Z. Zhang, S. Xu, Y.F. Wang, Q.L. Dai, B. Dong, L. Xu, H.W. Song, Inhibited local thermal effect in upconversion luminescence of YVO$_4$:Yb^{3+}, Er^{3+} inverse opals, Opt. Express 20 (2012) 29673–29678.

[7] M.C. Gonçalvesa, L.M. Fortesa, R.M. Almeidaa, A. Chiaserab, A. Chiappinib, M. Ferrarib, 3-D rare earth-doped colloidal photonic crystals, Opt. Mater. 31 (2009) 1315–1318.

[8] B. Hatton, L. Mishchenko, S. Davis, K.H. Sandhage, J. Aizenberg, Assembly of large-area, highly ordered, crack-free inverse opal films, Proc. Natl. Acad. Sci. USA 107 (2010) 10354–10359.

[9] T. Yoshie, A. Scherer, J. Hendrickson, G. Khitrova, H.M. Gibbs, G. Rupper, C. Ell, O.B. Shchekin, D.G. Deppe, Vacuum Rabi splitting with a single quantum dot in a photonic crystal nanocavity, Nature 432 (2004) 200–203.

[10] E. Yablonovitch, Inhibited spontaneous emission in solid-state physics and electronics, Phys. Rev. Lett. 58 (1987) 2059–2060.

[11] S. John, Strong localization of photons in certain disordered dielectric superlattices, Phys. Rev. Lett. 58 (1987) 2486–2849.

[12] N. Sui, Y.H. Wang, Y.F. Song, F.Y. Wang, Y.G. Ma, H.Z. Zhang, Manipulating fluorescence characteristics of conjugated fluorescent molecules incorporated into three-dimensional poly(methyl methacrylate) opal photonic crystals, Appl. Phys. Express 7 (2014) 025202.

[13] C. Qian, Y.H. Wang, Y.F. Song, L. Zou, Y.G. Ma, Y.Q. Yang, H.Z. Zhang, Modulation of spontaneous emission characteristics of Alq3 in three-dimensional PMMA photonic crystals, J. Polym. Sci. Part B: Polym. Phys. 52 (2014) 842–847.

[14] D.K. Hwang, H. Noh, H. Cao, R.P.H. Chang, Photonic bandgap engineering with inverse opal multistacks of different refractive index contrasts, Appl. Phys. Express 95 (2009) 091101.

[15] S.Y. Lin, J.G. Fleming, D.L. Hetherington, B.K. Smith, R. Biswas, K.M. Ho, M. Sigalas, W. Zubrzycki, S.R. Kurtz, J. Bur, A three-dimensional photonic crystal operating at infrared wavelengths, Nature (London) 394 (1998) 251–253.

[16] S. Noda, K. Tomoda, N. Yamamoto, A. Chutinan, Full three-dimensional photonic bandgap crystals at near-infrared wavelengths, Science 289 (2000) 604–606.

[17] S. Kawakami, O. Hanaizumi, T. Sato, Y. Ohtera, T. Kawashima, N. Yasuda, Y. Takei, K. Miura, Fabrication of 3D photonic crystals by autocloning and its applications, Electron Commun. Jpn. Part 2: Electron 82 (1999) 43–52.

[18] M. Campbell, D.N. Sharp, M.T. Harrison, R.G. Denning, A.J. Turberfield, Fabrication of photonic crystals for the visible spectrum by holographic lithography, Nat. (Lond.) 404 (2000) 53–56.

[19] K. Aoki, H.T. Miyazaki, H. Hirayama, K. Inoshita, T. Baba, K. Sakoda, N. Shinya, Y. Aoyagi, Microassembly of semiconductor three-dimensional photonic crystals, Nature Mater. 2 (2003) 117–121.

[20] M. Deubel, G. Von Freymann, M. Wegener, S. Pereira, K. Busch, C.M. Soukoulis, Direct laser writing of three-dimensional photonic-crystal templates for telecommunications, Nat. Mater. 3 (2004) 444–447.

[21] V.N. Astratov, V.N. Bogomolov, A.A. Kaplyanskii, A.V. Prokofiev, L.A. Samoilovich, S.M. Samoilovich, Yu. A. Vlasov, Optical spectroscopy of opal matrices with CdS embedded in its pores: quantum confinement and photonic band gap effects, IL Nuovo Cimento D 17 (1995) 1349–1354.

[22] Y.A. Vlasov, K. Luterova, I. Pelant, B. Hönerlage, Enhancement of optical gain of semiconductors embedded in three-dimensional photonic crystals, Appl. Phys. Lett. 71 (1997) 1616–1618.

[23] P. Lodal, A.F. van Driel, S. Nikolaev, A. Irman, K. Overgaag, D. Vanmaekelbergh, W.L. Vos, Controlling the dynamics of spontaneous emission from quantum dots by photonic crystals, Nature 430 (2004) 654–657.

[24] Y.S. Zhu, W. Xu, H.Z. Zhang, W. Wang, S. Xu, H.W. Song, Inhibited long-scale energy transfer in dysprosium doped yttrium vanadate inverse opal, J. Phys. Chem. C 116 (2012) 2297–2302.

[25] I.S. Nikolaev, P. Lodahl, A.F. van Driel, A.F. Koenderink, W.L. Vo, Strongly nonexponential time-resolved fluorescence of quantum-dot ensembles in three-dimensional photonic crystals, Phys. Rev. B 75 (2007) 115302.

[26] A.F. van Driel, I.S. Nikolaev, P. Vergeer, P. Lodahl, D. Vanmakekelbergh, W.L. Vos, Statistical analysis of time-resolved emission from ensembles of semiconductor quantum dots: interpretation of exponential decay models, Phys. Rev. B 75 (2007) 035329.

[27] D. Valerini, A. Creti, M. Lomascolo, L. Manna, R. Cingolani, M. Anni, Temperature dependence of the photoluminescence properties of colloidal CdSe/ZnS core/shell quantum dots embedded in a polystyrene matrix, Phys. Rev. B 71 (2005) 235409.

[28] B.H. Chon, J. Bang, J. Park, C. Jeong, J.H. Choi, J.B. Le, T. Joo, S. Kim, Unique temperature dependence and blinking behavior of cdte/cdse (core/shell) type-ii quantum dots, J. Phys. Chem. C 115 (2011) 436–442.

[29] Y.P. Varshni, Temperature dependence of the energy gap in semiconductors, Physica 34 (1967) 149–154.

[30] H.Y. Fan, Temperature dependence of the energy gap in semiconductors, Phys. Rev. 82 (1951) 900–905.

[31] V.I. Klimov, A.A. Mikhailovsky, D.W. McBranch, C.A. Leatherdale, M.G. Bawendi, Quantization of multiparticle auger rates in semiconductor quantum dots, Science 287 (2000) 1011–1103.

[32] V.I. Klimov, Optical nonlinearities and ultrafast carrier dynamics in semiconductor nanocrystals, J. Phys. Chem. B 104 (2000) 6112–6123.